HHS Public Access

Author manuscript

Antiviral Res. Author manuscript; available in PMC 2020 February 04.

Published in final edited form as:

Antiviral Res. 2019 February ; 162: 61–70. doi:10.1016/j.antiviral.2018.11.012.

Development of a Respiratory Disease Model for Enterovirus D68 in 4-Week-Old Mice for Evaluation of Antiviral Therapies

W. Joseph Evans[a,b,d], **Brett L. Hurst**[a,b,d], **Christopher J. Peterson**[a,b], **Arnaud J. Van Wettere**[a,b,c], **Craig W. Day**[a,b], **Donald F. Smee**[a,b], **E. Bart Tarbet**[a,b,c,*]

[a]Institute for Antiviral Research, Utah State University, Logan, UT

[b]Department of Animal, Dairy and Veterinary Sciences, Utah State University, Logan, Utah

[c]Utah Veterinary Diagnostic Laboratory, Logan, Utah.

[d]W.J.E. and B.L.H. contributed equally to this manuscript.

Abstract

Enterovirus D68 (EV-D68) is a non-polio enterovirus that affects the respiratory system and can cause serious complications, especially in children and older people with weakened immune systems. As an emerging virus, there are no current antiviral therapies or vaccines available. Our goal was to develop a mouse model of human EV-D68 infection that mimicked the disease observed in humans and could be used for evaluation of experimental therapeutics. This is the first report of a respiratory disease model for EV-D68 infection in mice. We adapted the virus by 30 serial passages in AG129 mice, which are deficient in IFN- α/β and –γ receptors.

Despite a lack of weight loss or mortality in mice, lung function measured by plethysmography, showed an increase in enhanced pause (Penh) on days 6 and 7 post-infection. In addition, as virus adapted to mice, virus titer in the lungs increased 320-fold, and the pro-inflammatory cytokines MCP-1 and RANTES increased 15-fold and 2-fold in the lung, respectively. In addition, a time course of mouse-adapted EV-D68 infection was determined in lung, blood, liver, kidney, spleen, leg muscle, spinal cord and brain. Virus in the lung replicated rapidly after intranasal inoculation of adapted virus, 10^6 $CCID_{50}$/mL by 4 hours and $10^{8.3}$ $CCID_{50}$/mL by 24 hours. Virus then spread to the blood and other tissues, including spinal cord and brain. This mouse model for EV-D68 infection includes enhanced pause (Penh) as an indicator of morbidity, and viremia, virus titers and proinflammatory cytokines in the lung, and lung histopathology as indicators of disease. Our mouse-adapted virus has a similar antiviral profile to the original isolate as well as another respiratory picornavirus, rhinovirus-14. This model will be valuable in evaluating experimental therapies in the future.

*Corresponding Author: E. Bart Tarbet, Utah State University, Logan, Utah, 84322-5600 bart.tarbet@usu.edu, Tel: 1 (435) 797-3954.

7 Conflicts of Interest

The authors declare no conflict of interest.

Keywords

Enterovirus D68; Respiratory Disease; Animal Model; AG129 mice

1. Introduction

According to the Centers for Disease Control and Prevention (CDC), enteroviruses cause about 15 million infections annually in the United States. Most people infected with enterovirus are asymptomatic or have only mild illness (Midgley et al., 2014). However individuals with asthma or reactive airway disease (Midgley et al., 2014; Midgley et al., 2015), infants and/or individuals with weakened immune systems can have serious complications when infected with EV-D68 (Smee et al., 2016). EV-D68 infections were rarely reported after their initial discovery in 1962 (Imamura and Oshitani, 2015). However, since the early 2000's EV-D68 has been increasing in prevalence as a cause of respiratory illness.

In 2014, the United States experienced an outbreak of Enterovirus D68 with over 1,100 cases reported (Rhoden et al., 2015). The cases were mostly children with severe respiratory illness (Imamura and Oshitani, 2015). Enterovirus D68 patients presented with shortness of breath, cough, and nasal congestion. Patients also showed decreased air entry or wheezing, and moderate to severe respiratory distress. In addition, 5-10% of individuals who tested positive for EV-D68 exhibited neurological disease (Imamura et al., 2015). Two states, Colorado and California originally reported these cases of acute flaccid paralysis (AFP). However, by mid-December at least 33 states in the U.S. reported children with AFP who were positive for EV-D68 (Greninger et al., 2015; Matsumoto et al., 2016; Messacar et al., 2016; Messacar et al., 2015).

To date there are no approved treatments for EV-D68, although there are many compounds that have shown efficacy against EV-D68 *in vitro*, including Rupintrivir, Enviroxime and Pleconaril (Rhoden et al., 2015; Smee et al., 2016; Sun et al., 2015). One reason treatments have not been approved is that until recently, an animal model for study of experimental therapeutics against EV-D68 was not available. A cotton rat infection model was recently reported using non-adapted EV-D68 (Patel et al., 2016). In addition, a model was recently developed showing the neurotropic effects of EV-D68 in neonatal Swiss Webster mouse pups (Hixon et al., 2017). However, this is the first report of a respiratory disease model for EV-D68 infection in mice. Unlike other models, we developed an EV-D68 model by adapting the virus to AG129 mice through serial passage. We demonstrate that the mouse-adapted EV-D68 replicated rapidly in the lung after intranasal inoculation of virus, and then spread to the blood and other tissues, including spinal cord and brain.

2 Materials and Methods

2.1 Viruses and Cell Lines.

The following viruses were obtained from the American Type Culture Collection (ATCC, Manassas, VA): enterovirus D68 (US/MO/14-18949) and human rhinovirus type 14 (RV-14).

Human rhabdomyosarcoma (RD) cells were obtained from ATCC. HeLa-Ohio-1 (human cervical epithelioid carcinoma) cells were obtained from Dr. Frederick Hayden (University of Virginia, Charlottesville, VA). Media used for EV-D68 cell culture infection included 2% FBS and 25 mM $MgCl_2$ in MEM + 50 μg/ml of gentamicin. Tissues harvested from mice were homogenized in MEM.

2.2 Animals.

Male and female AG129 mice, deficient in IFN- α/β and –γ receptors (Muller et al., 1994; van den Broek et al., 1995), were obtained from a specific-pathogen free breeding colony at Utah State University. For model development, male and female mice were used in all studies.

2.3 Passage of virus in mice.

Four-week-old AG129 mice were used to serially-passage Enterovirus D68 (US/MO/14-18949) (Smee and Barnard, 2013). For each passage, the animals were infected intranasally with EV-D68. After three days, lungs from infected mice were homogenized in 1 mL of MEM. Part of the recovered virus was titrated on human RD cells and part of the lung homogenate was pooled and used to re-infect the next group of mice. This was repeated for 30 passages. A modified CDC RT-PCR protocol was used to verify that samples from each mouse passage contained EV-D68 (Wylie et al., 2015). The mouse-passaged (MP) virus was labeled sequentially as MP1, MP2, etc.

2.4 Virus Titration Assay.

Microtiter plates were seeded with RD cells 24 hours prior to infection and incubated at 37°C with 5% CO_2. Samples collected from mouse tissues were serially diluted, and 10-fold dilutions added to microtiter plates and incubated for 6 days at 33°C with 5% CO_2 (Smee et al., 2016). Six days post-infection (p.i.), cells were examined visually for viral cytopathic effect. The 50% cell culture infectious dose ($CCID_{50}$) was calculated using an endpoint dilution method (Reed LJ, 1938).

2.5 Plaque Purification of Mouse Passage 30 (MP30pp) virus.

EV-D68 MP30 was serially diluted and plated onto 12-well microplates containing RD cells. The virus was incubated with cells for 1-hour, the growth medium was removed and replaced with 0.6% SeaPlaque™ Agarose (FMC Bioproducts, Rockland, ME USA), 2% FBS and 25mM $MgCl_2$. Cells were observed for plaques until day 3 day p.i.. Individual plaques were selected and inoculated into T-25 flasks containing RD cells and growth media. Virus from T-25 flasks showing 100% CPE after 2-3 days was harvested and used to repeat the plaque purification procedure three times. The resulting virus stock was labeled MP30pp.

2.6 Comparison of Mouse Passaged Viruses.

To demonstrate the effects of virus adapted over the 30 passages, five groups of mice were infected with MP0, MP10, MP20, MP30, and MP30pp. Mouse tissues (lungs, liver, kidneys,

spleen and whole blood) were harvested from mice on day three p.i. and virus titers determined on RD cells.

2.7 Time Course of Infection.

The time course of infection following i.n. administration of mouse-adapted EV-D68 (MP30pp) included collection of mouse tissues for evaluation of virus titers. Tissues including: lungs, liver, kidney, spleen, blood, spinal cord, brain and leg muscle, were harvested at 8 hours and day 1, 3, 5, 7, 9 p.i. At each time point, mice were euthanized and tissues collected for virus titers, histological analyses, and measurement of pro-inflammatory cytokines in the lung.

2.8 Histological analyses.

The left lung, liver, kidney and spleen were removed and fixed in 4% paraformaldehyde for 2 days. Paraformaldehyde-fixed tissue sections were processed and embedded in paraffin by standard techniques. Sections, 5 μm thick, were stained with hematoxylin and eosin (H&E) and examined by light microscopy. A lesion severity grading system was used: 0 = no lesion, 1+ = minimal lesion, 2+ = mild lesion, 3+ = moderate lesion and 4+ = severe lesion.

Infected (EV-D68 MP30pp $10^{6.5}$ $CCID_{50}$/mouse) and sham infected mice were sacrificed on day 2 post-infection. Mice were perfused transcardially with phosphate buffered saline (PBS) followed by 4% paraformaldehyde. Lungs were removed and post-fixed in the same fixative for 2 days. All tissues were cryoprotected in 30% sucrose in PBS for 3 days at 4 °C, embedded in OCT compound (Ted Pella, Inc), and frozen in a dry ice/isopentane bath. Eight sets of adjacent 30 μm sections were cut by cryostat, mounted on slides, and stored at 4 °C until ready for additional processing. For immunohistofluorescence staining, sections were dried on a slide warmer (Lab Line, Midland, ON, Canada) at 50 °C, then encircled with a hydrophobic barrier pen (ImmEdge, Vector Labs), rinsed with PBS, and covered in blocking solution (10% normal serum, 0.5% Triton X-100 in PBS) for 1 hour (hr). Primary antibody against EV-D68 VP2 capsid protein (GeneTex, GTX132314, Irvine, CA) was diluted 1/100 in antibody blocking solution (10% normal serum, 0.2% Triton X-100 in PBS) and added to sections for incubation overnight at room temperature. Secondary antibodies conjugated to Alexa-488 (ThermoFischer Scientific) were diluted 1/200 in antibody blocking solution. Sections were rinsed three times in PBS, incubated with secondary antibody solution for 2 hr at room temperature, and rinsed twice in PBS. Coverslips were mounted with Fluoromount G (Southern Biotech, Birmingham, AL).

2.9 Imaging and image processing.

Fluorescent images were obtained at 200X with a laser scanning confocal microscope (Zeiss, LSM710). For images chosen for publication, settings were adjusted to maximize the signal-to-noise ratio so that relevant features could be seen more clearly. The same settings were used for each image.

2.10 Lung Cytokine/Chemokine Evaluations.

A sample (200 μl) from each lung homogenate was tested for cytokines and chemokines using a chemiluminescent assay according to the manufacturer's instructions (Quansys

Biosciences Q-Plex™ Array, Logan, UT). The Quansys multiplex ELISA is a quantitative test in which 16 distinct capture antibodies are applied to each well of a 96-well plate in a defined array. Each sample supernatant was tested at 2 dilutions for the following: IL-1α, IL-1β, IL-2, IL-3, IL-4, IL-5, IL-6, IL-10, IL-12p70, IL-17, MCP-1, IFN-γ, TNFα, MIP-1α, GM-CSF, and RANTES. Cytokine and chemokine concentrations are reported as fold changes compared to measurements from uninfected control mice (baseline). Definition of abbreviations are: IL - interleukin; MCP - monocyte chemoattractant protein; IFN - interferon; TNF - tumor necrosis factor, MIP – macrophage inflammatory protein; GM-CSF - granulocyte/ macrophage colony stimulating factor; and RANTES - regulated upon activation, normal T cell expressed and secreted.

2.11 Evaluation of Lung Function by Plethysmography.

The plethysmograph and mouse-sized acquisition chambers (emka Technologies, Falls Church, VA) were used to evaluate lung function. The following parameters were measured and analyzed: enhanced pause (Penh), tidal volume (TV), minute volume (MV) and expiratory volume (EV), times of inspiration (Ti), expiration (Te), and relaxation (RT), peak inspiratory (PIF) and expiratory (PEF) flow, frequency of breath (Freq), 50% expiratory flow (EF50) and end inspiratory (EIP) and expiratory (EEP) pauses. To reduce variability, mean readings from infected mice were normalized to mean readings from sham-infected (cell culture medium) controls on each day. To obtain measurements, mice were placed in the chambers and allowed to acclimate for three minutes. Plethysmography readings were then recorded for the next five minutes in response to room air. To simulate a hypercapnia challenge, the chambers were flooded with a gas mixture containing 7% CO_2, 50% O_2 and balanced with N_2. The plethysmography readings were recorded for an additional five minutes as CO_2-challenged.

2.12 Antiviral Compounds.

Enviroxime was obtained from the U.S. Army Medical Research Institute of Infectious Diseases (USAMRIID), Ft. Detrick, Frederick, MD through the NIAID antiviral screening program. Pirodavir was purchased from AdooQ Bioscience, (Irvine, CA). Pleconaril was obtained from the former Biota Pharmaceuticals (Notting Hill, Victoria, Australia). Rupintrivir and Guanidine HCl were purchased from Sigma Aldrich (St. Louis, MO).

2.12 *In Vitro* Antiviral Assays.

In vitro antiviral studies were conducted by the inhibition of virus-induced cytopathic effect in triplicate wells of 96-well microplates of infected cells as described previously (Barnard et al., 2004; Smee et al., 2016). EV-D68 viruses were evaluated in RD cells at 33°C with 25 mM $MgCl_2$ and 2% FBS in MEM. RV-14 was evaluated in Hela-Ohio cells at 33°C with 25 mM $MgCl_2$ and 2% FBS in MEM. The percentage of viral destruction was quantified by neutral red dye uptake. Compounds were evaluated at 8 half-log_{10} concentrations designed to bracket the 50% virus inhibitory concentration (EC_{50}). The 50% cytotoxic concentrations (CC_{50}) of the compounds were determined in duplicate uninfected wells on the same microtiter plate. A selectivity index (SI) was calculated for each compound by dividing the CC_{50} by the EC_{50}.

2.14 RNA isolation, PCR amplification and sequencing of mouse adapted virus

Viral RNA was isolated from virus-infected cell culture supernatant by using a Qiamp Viral RNA Mini Kit (Qiagen, Germantown, MD) according to the manufacturer's protocol. Primers were generated for three sets of overlapping consensus sequences to mimic the protocol employed by the Centers for Disease Control and Prevention (Ng et al., 2016). The EV-D68 genome was divided into three amplicons. The first ampliconwas from the 50UTR to VP1 (CCACTCCAAGGGCCCACGTG [1e20]; TCGTGAGTATAGTGATCTCAGCATCAAATCTAAGGTAT [2737-2700]), the second from VP1 to 2C (TGTGGTCCCTAGCTTAAATGCAGTTGAAAC [2430- 2359]; ACTATTAGCTCATTTGATGGGTGTACTACAATCCA [5147- 5113]), and the third from 2C to 30UTR (GGATTCTCAAGAAGTTAGGGATTATTGCCAAAAGAAAG [5073e5110]; GGTTCCCAATTAAACGAAAATTTACCTCTAAATGAAAGTAAC [7311- 7270]). All primers were based off coordinates for EV-D68 US/ MO/14e18949 (Genbank KM851227.1). cDNAwas generated using a Superscript™ First-Strand Synthesis System (Thermo Fisher Scientific, Waltham, MA). A virus-specific reverse primer generated from the sequence of the 30UTR region of EV-D68 was used for firststrand synthesis. cDNA samples were used as the template for PCR with Thermo Scientific Phusion High-Fidelity DNA Polymerase (Thermo Fisher Scientific, Waltham, MA) using the manufacturer's 3-step protocol. For each sample, all three amplicons were pooled and purified using the Nucleospin® Gel and PCR Clean-up kit (Macherey-Nagel, Bethlehem, PA). Samples were submitted to the DNA Sequencing Core (University of Utah, Salt Lake City, UT) for analysis on their Ion Torrent Next Generation Sequencing (NGS) Technology. Sequence data was aligned using the EV-D68 US/MO/ 14e18949 sequence as the reference genome using the Integrative Genomics Viewer (Robinson et al., 2011; Thorvaldsdottir et al., 2013). Individual nucleotide mutations were recorded for each sample. Changes to the amino acid sequence were determined using the Translate Tool on the ExPASy resource portal from the Swiss Institute for Bioinformatics (www.sib.swiss/). Protein sequences were aligned for mutations using the Protein BLAST tool from the National Center for Biotechnology Information (www.ncbi.nlm.nih.gov/). As the amino acid sequence was not determined experimentally, all changes to amino acids are predicted based upon the nucleotide sequence.

2.15 Ethical Treatment of Animals.

This study was completed under the approval of the Institutional Animal Care and Use Committee of Utah State University. The work was performed in the AAALAC-accredited Laboratory Animal Research Center of Utah State University in accordance to the National Institutes of Health Guide for the Care and Use of Laboratory Animals (National Research Council (U.S.) Committe for the Update of the Guide for the Care and Use of Laboratory Animals, 2011).

2.16 Statistical Analysis.

Statistical Analysis was completed using Prism 7.0d, Graph Pad Software (San Diego, CA). For comparison of virus titers, a one-way analysis of variance (ANOVA) followed by Tukey’s multiple comparison, or by two-way ANOVA was used for effects based on the day

p.i. using Prism 7.0d. Group differences in histologic lesion scores were determined by Kruskal-Wallis non-parametric test, followed by Dunn's multiple comparison test using Prism 7.0d. Cytokine and chemokine measurements were compared by ANOVA assuming equal variance and normal distribution.

3 Results

3.1 Comparison of Mouse Passaged EV-D68.

A comparison of EV-D68 after mouse passaging determined which virus passage produced the highest virus titers and greatest disease signs for the model (Figure 1). Virus titers in whole blood were at the limit of detection of the assay for MP0, and then increased from $10^{1.33}$ to $10^{2.5}$ $CCID_{50}$ per mL for MP10 and MP30 (Figure 1A). Virus recovered from the lungs of infected mice increased from $10^{5.8}$ to $10^{7.0}$ $CCID_{50}$ per mL for MP0 and MP10, respectively, then remained nearly constant at $10^{7.3}$ $CCID_{50}$ per mL for MP10 through MP30 (Figure 1B). Virus titers in liver samples were at the limit of detection for MP0, then increased from $10^{3.0}$ to $10^{3.5}$ for MP10 and MP20, and MP30 was 100-fold higher at $10^{5.5}$ $CCID_{50}$ per mL. In addition, virus titers in Kidney increased from $10^{1.5}$ to $10^{5.2}$ $CCID_{50}$ per mL for MP0 to MP30, and in spleen from $10^{1.5}$ to $10^{4.8}$ $CCID_{50}$ per mL for MP0 to MP30.

During adaptation of EV-D68 to mice, we did not observe weight loss or mortality following infection. Therefore, we sought to identify other parameters that could indicate virus was adapting and producing an infection in mice. Virus titers in lung tissues was a primary marker for virus adaptation, but we also observed an increase in the proinflammatory cytokines, MCP-1 and RANTES. This was an early indication that EV-D68 was adapting to infect mice, as the infection was inducing an inflammatory response. Figure 2 shows MCP-1 and RANTES concentrations in lung following infection with EV-D68 at different passage numbers. Lung samples from mice infected with EV-D68 MP0, MP10, MP20, MP30, and MP30pp were evaluated by multiplex ELISA for a panel of 16 pro-inflammatory cytokines and chemokines. Mice infected with MP0 showed similar concentrations of cytokines to those of uninfected control mice. However, the pro-inflammatory cytokines MCP-1 and RANTES showed significant increases in groups infected with MP10, MP20, MP30 and MP30pp as virus adapted to mice (Figure 2). The mice infected with MP30 showed the highest levels of MCP-1 and RANTES. The mice infected with MP30pp also showed higher levels of MCP-1 than the mice infected with MP0, MP10, and MP20. However, RANTES levels decreased with the plaque purified strain of virus compared to MP30 (Figure 2). Pro-inflammatory cytokines from other tissues were evaluated, although significant differences compared to control mice were not observed (data not shown).

Histopathology revealed lesions of interstitial pneumonia in the lung that increased in severity as EV-D68 was passaged in mice from MP0 to MP30 (Figure 3). Even though lung virus titers, RANTES levels, and pneumonia severity grades appeared to be slightly lower after plaque purification of MP30, we considered a plaque-purified virus to be essential for qualification of our EV-D68 mouse model.

3.2 Time Course of Infection with mouse-adapted EV-D68.

Mice receiving the highest challenge dose ($10^{6.5}$ $CCID_{50}$) showed peak virus titers on day 1 for lung, liver, and spleen, and on day 3 for kidney (Figure 4). At 4 hours p.i. 10^{6} $CCID_{50}$ virus per mL was recovered from lung tissues, by 8-hours p.i. the virus titers increased to $10^{7.7}$ $CCID_{50}$/mL and by 24 hours (day 1) the titer was $10^{8.3}$ $CCID_{50}$/mL. The titer remained high through day 3 p.i., then decreased on day 5 and was undetectable by day 9. The lower dose challenge groups showed peak titers on day 3 that decreased on day 5 p.i. and were undetectable by day 7 p.i. (Figure 4).

Blood, spinal cord, brain and leg muscle tissues were only collected from mice infected with highest ($10^{6.5}$ $CCID_{50}$) and lowest ($10^{4.5}$ $CCID_{50}$) challenge doses (Figure 5). Mice receiving the high dose challenge showed peak virus titers on day 1 for blood and brain, day 3 for leg muscle, and days 1-3 for spinal cord. The lower dose challenge showed peak titers on day 3 or 5 (Figure 5). Of note, was the rapid appearance of virus in the CNS (spinal cord and brain tissues) in mice infected with the high challenge dose (Figure 5). These results indicate that EV-D68 infection in the mouse becomes systemic and replicates at multiple sites (Figure 4 and 5). Virus titers in the blood were lower than other tissues, and cleared more rapidly, suggesting that virus is replicating in the tissues and not coming from blood remaining in those tissues. In addition, we considered the possibility that virus was gaining access to the CNS by retrograde axonal transport from peripheral nerves in the leg, so observation of virus in leg muscle was important to ascertain.

3.3 Identification of EV-D68 in lung tissues following infection with EV-D68.

All mice infected with EV-D68 MP30pp showed a moderate interstitial pneumonia characterized by perivascular and alveolar wall infiltration with mononuclear inflammatory cells. Lungs from infected and sham-infected mice were harvested at day 2 post-infection for immunofluorescence staining (IFA) with antibodies directed to EV-D68 VP2 capsid protein. Immunoreactivity was observed in lung tissue from infected mice (Figure 6). Samples from liver, kidney and spleen were also evaluated by IFA, but histological lesions were not observed (data not shown). The entire tissue sample containing spinal cord, brain and leg muscle were used to obtain virus titers, therefore these samples were not evaluated by IFA.

3.4 Lung cytokines/chemokines following infection with EV-D68.

Pro-inflammatory cytokines and chemokines in lung samples were evaluated by multiplex ELISA after infection with mouse-adapted EV-D68. Following infection with the highest dose of EV-D68 ($10^{6.5}$ $CCID_{50}$/mouse), all cytokines and chemokines increased on day 1 p.i., except for IL-17 (Supplementary Figures S1 to S4). MCP-1 and IL-6 showed the greatest change compared to uninfected controls (baseline), with 48-fold and 140-fold increases, respectively. In addition, IL-1β, IL-2, and IL-5 increased between 10-fold and 20-fold compared to baseline (Supplementary Figures S1 to S4). This rapid response is characteristic of EV-D68 infections and has been described for the cotton rat by Patel et al. (2016). Several cytokines, including IL-1β, IL-2, IL-4, IL-17, and GM-CSF showed significant increases on day 5 p.i. following challenge with the low dose challenge, and may represent a challenge dose effect (Supplementary Figures S1 to S4).

3.5 Lung function parameters following infection with EV-D68.

To develop a practical model for evaluation of antiviral therapeutics, we determined disease signs that would not require sacrifice of infected mice. Julander, et al. previously described the use of plethysmography for evaluation of lung function following respiratory virus infection in the mouse (Julander, 2011). Therefore, we used plethysmography to assess lung function after mouse-adapted EV-D68 infection. Four groups of eight mice (4 males and 4 females per group) were used to evaluate the impact of EV-D68 infection on lung function as measured by plethysmography. A sham-infected group was used as baseline for plethysmography measurements. In this study, mice receiving highest dose of EV-D68 showed an increase in Penh on days 6 and 7 compared to baseline (Figure 7). Penh has been identified as a measure of airway distress (Julander et al., 2011; Loddo et al., 1962). We consider the increase in Penh as an indicator of morbidity following infection, which is in agreement with the increased lesion scores and cytokine concentrations observed in the lung after EV-D68 infection. Several additional parameters of lung function showed significant differences from controls in this study, including decreases in expiratory time on days 2-7, increases in minute volume on days 6-7, and increases in frequency on days 2-6 (Supplementary Figures S5 to S7). However, only Penh showed consistent increases following EV-D68 infection in multiple studies.

3.6 In vitro antiviral comparison.

Because of similarities between EV-D68 and rhinoviruses, including their replication temperature in cell culture (Oberste et al., 2004), acid-lability (Oberste et al., 2004), and the fact that both types of virus cause respiratory disease (Foster et al., 2015; Zheng et al., 2017), we hypothesized that this new mouse model for EV-D68 could also be used as a model for rhinovirus infections. In addition, we previously reported the similarity in the *in vitro* antiviral activity profile between EV-D68 and rhinovirus 87 (Smee et al., 2016). However, after publication of those data, we learned that rhinovirus 87 had been reclassified as enterovirus D68 (Palmenberg and Gern, 2015). Therefore, we completed another *in vitro* antiviral comparison using EV-D68 MP0 (non-adapted), MP30PP and rhinovirus 14 (RV-14) to determine if our hypothesis held any merit as to the potential application of this mouse model for rhinoviruses. The results from this *in vitro* antiviral comparison are shown in Table 1. Rupintrivir was the most effective against the three viruses with selectivity indices ($SI = CC_{50} / EC_{50}$) of >3333, >2500, and >333, respectively. Enviroxime and pleconaril were also highly active with selectivity indices between 23.2 and 131 against the three viruses. Guanidine, a known inhibitor of poliovirus (Loddo et al., 1962), was previously evaluated against strains of EV-D68 and shown to be highly active (Smee et al., 2016). That antiviral activity was confirmed against EV-D68 MP0 and the mouse-adapted EV-D68 MP30pp virus with selectivity indices of 31.7 and 23.3 against the two EV-68 viruses, and 37.6 against rhinovirus 14. Following mouse adaptation of EV-D68 the selectivity index decreased for Enviroxime, Guanidine and Rupintravir.

3.7 Nucleotide and predicted amino acid changes in the mouse adapted EV-D68 virus

The complete sequence of the mouse-adapted virus (MP30PP) was submitted to GenBank (Accession Number MH708882). Adaptation of the EV-D68 virus to the lungs of AG129

mice produced a total of 22 amino acid changes, nine of which are predicted to produce changes in the amino acid sequence of the EV-D68 proteins. A summary of nucleotide and predicted amino acid changes is shown in Table 2. One amino acid change is predicted in the VP4 protein, two in the VP3 protein, four in the VP1 protein, one in the 2A protein, and one in the 3D protein. A visual representation of these amino acid changes in relation to the EV-D68 genome is shown in Fig. 8. In addition, five nucleotide changes were detected in the 50 untranslated region (50UTR) corresponding to the highly conserved internal ribosome entry site (IRES).

4 Discussion

To develop antiviral therapies and vaccines for EV-D68 infections, use of an animal model is critical. Recently, three models have been described. The first model takes advantage of the abundance of α2,6 linked sialic acid receptors in the respiratory system of the cotton rat (Patel et al., 2016). In this model, using non-adapted EV-D68, Patel et al. (2016)showed a “mild cumulative pathology” in the lungs (Matsumoto et al., 2016; Patel et al., 2016). In addition, MCP-1 peaked at 4-hours post-virus exposure using the VANBT/1 strain of EV-D68 (Patel et al., 2016). However, after the initial peak, cytokine levels decreased rapidly.

A second model utilized neonatal Swiss-Webster mice (Hixon et al., 2017). In this model, five different strains of EV-D68 were shown to induce limb paralysis and death in two-day-old mouse pups following intracerebral injection of virus. This model provides evidence that EV-D68 infection can cause neurological disease. In addition, Hixon et al. (2017) demonstrated that serum containing EV-D68 antibodies was able to confer immunity to mice following treatment with serum 1 day prior to infection (Oberste et al., 2004).

The third model utilized ferrets infected intranasally with the Fermon strain of EV-D68. EV-D68 was observed in nasal washes, throat swabs, blood, lymph node, lungs, and feces by qPCR (Zheng et al., 2017). In addition, EV-D68 caused a respiratory infection as seen in the lower respiratory tract by histological analysis (Flaño et al., 2009).

This is the first report of a respiratory disease model for EV-D68 infection in mice. The model developed in our laboratory demonstrates an increased ability of mouse-adapted virus to infect 4-week old AG129 mice. In addition, the model shows rapid replication of virus in the lungs and spread to blood and other tissues in the mouse. These results are consistent with the acute nature of human infections (Martin et al., 2016; Matsumoto et al., 2016; Schuster et al., 2015). In addition, the longest average stay for patients in the hospital was 4.75 days (Foster et al., 2015), suggesting an uncomplicated EV-D68 infection replicates and spreads rapidly, and then resolves in about one week. Our model also uses the natural route of infection and is more amenable to the evaluation of antiviral therapies. The cotton rat model requires intrathecal injection and the Swiss-Webster mouse model requires neonatal mice that are difficult to work with. In addition, the ferret model is costly and not available in many laboratories.

Following intranasal inoculation of mouse-adapted EV-D68, virus replicates to high titers in the lung and spreads rapidly to the blood and other tissues, including the CNS, suggesting

that EV-D68 is capable of causing neurological disease along with the respiratory disease. In addition, we observed altered lung function (Penh) following infection with mouse-adapted EV-D68, and an increase in proinflammatory cytokines in the lung, especially MCP-1 and IL-6, indicative of an active infection following challenge. Despite early viral replication and cytokine responses, an increase in Penh was not observed until days six and seven post-infection. We suspect that viral replication and the cytokine response are leading to pathological changes which are then observed in the Penh response. By day nine, virus titers were no longer detected in lung tissue and permanent lung tissue damage was not observed with histopathology.

Since EV-D68 shares biological features with both enteroviruses and rhinoviruses including their replication temperature in cell culture (Oberste et al., 2004), acid-lability (Oberste et al., 2004), both types of virus cause respiratory disease (Foster et al., 2015; Zheng et al., 2017), and similarity in the *in vitro* antiviral activity profile (Smee et al., 2016). Since no practical mouse models for human rhinovirus infections are available (Bartlett et al., 2015), we suggest that this model for EV-D68 respiratory disease may also serve as a model for rhinovirus infections. In addition, as vaccines for rhinoviruses have been difficult to develop, antiviral therapies may play a larger role in patient treatment. Therefore, future studies will evaluate antiviral therapies in this model for EV-D68 infection and potentially for rhinovirus 14.

Mouse-adaptation caused 22 nucleotide changes within the EVD68 genome, nine of which are predicted to result in amino acid changes. As may be expected, the majority of these predicted amino acid changes occur in the four structural proteins (VP1-VP4) of EVD68. Seven of the nine predicted amino acid changes are found within the EV-D68 structural proteins which may indicate a change in viral surface structure to utilize mouse cellular receptors. The effects of the other two predicted amino acid changes which occur in the 2A and 3D regions are less obvious. While the mutation in the 3D polymerase may assist viral replication in mouse cells, 2A protease is largely responsible for cleavage of the viral polyprotein into protein subunits.

In addition, future studies will determine if treatment regimens that reduce or prevent viremia can also prevent the onset of neurological signs following EV-D68 infection, as a concurrent manuscript describes the neurological model following intraperitoneal infection of mouse-adapted EV-D68 in 10-day-old AG129 mice (Hurst et al., 2019). In addition, sequence analyses of mouse-passaged virus has been initiated and will be published upon completion.

5 Conclusions

This is the first report of a respiratory disease model for EV-D68 infection in 4-week-old AG129 mice. This model has the potential for evaluation of antiviral therapies for EV-D68 infections. In addition, this model has well-established endpoints including; viremia, altered lung function (Penh), increase in virus titers and pro-inflammatory cytokines in lung tissues, and histological changes in the lung that can be used to evaluate the effectiveness of experimental antiviral drugs.

Supplementary Material

Refer to Web version on PubMed Central for supplementary material.

Acknowledgements

Funding for this research was provided by contract number HHSN272201000039I, Task Order A79, from the Virology Branch, Division of Microbiology and Infectious Diseases, National Institute of Allergy and Infectious Diseases, National Institutes of Health, USA.

References

Barnard DL, Hubbard VD, Smee DF, Sidwell RW, Watson KG, Tucker SP, Reece PA, 2004 In vitro activity of expanded-spectrum pyridazinyl oxime ethers related to pirodavir: novel capsid-binding inhibitors with potent antipicornavirus activity. Antimicrob Agents Chemother 48, 1766–1772. [PubMed: 15105133]

Bartlett NW, Singanayagam A, Johnston SL, 2015 Mouse models of rhinovirus infection and airways disease. Methods Mol Biol 1221, 181–188. [PubMed: 25261315]

Flaño E, Jewell NA, Durbin RK, Durbin JE. 2009 Methods used to study respiratory virus infection. Current protocols in cell biology / editorial board, Juan S Bonifacino. [Chapter:26.3].

Foster CB, Friedman N, Carl J, Piedimonte G. 2015 Enterovirus D68: a clinically important respiratory enterovirus. Cleve Clin J Med 82:26–31. [PubMed: 25552624]

Greninger AL, Naccache SN, Messacar K, Clayton A, Yu G, Somasekar S, Federman S, Stryke D, Anderson C, Yagi S, Messenger S, Wadford D, Xia D, Watt JP, Van Haren K, Dominguez SR, Glaser C, Aldrovandi G, Chiu CY. 2015 A novel outbreak enterovirus D68 strain associated with acute flaccid myelitis cases in the USA (2012-14): a retrospective cohort study. Lancet Infect Dis 15:671–682. [PubMed: 25837569]

Hixon AM, Yu G, Leser JS, Yagi S, Clarke P, Chiu CY, Tyler KL. 2017 A mouse model of paralytic myelitis caused by enterovirus D68. PLoS Pathog 13:e1006199. [PubMed: 28231269]

Hurst BL, Evans WJ, Smee DF, Van Wettere A, Tarbet EB 2019 Evaluation of Antiviral Therapies in Respiratory and Neurological Disease Models of Enterovirus D68 Infection in AG129 Mice. Virology 526:146–154. [PubMed: 30390563]

Imamura T, Oshitani H. 2015 Erratum: Global reemergence of enterovirus D68 as an important pathogen for acute respiratory infections. Rev Med Virol 25:268. [PubMed: 26151890]

Julander JG, Hagloch J, Latimer S, Motter N, Dagley A, Barnard DL, Smee DF, and Morrey JD. 2011 Use of plethysmography in assessing the efficacy of antivirals in a mouse model of pandemic influenza A virus. Antiviral Res 92:228–236. [PubMed: 21867731]

Loddo B, Ferrari W, Brotzu G, Spanedda A. 1962 In vitro inhibition of infectivity of polio viruses by guanidine. Nature 193:97–98. [PubMed: 14466152]

Martin G, Li R, Cook VE, Carwana M, Tilley P, Sauve L, Tang P, Kapur A, Yang CL. 2016 Respiratory Presentation of Pediatric Patients in the 2014 Enterovirus D68 Outbreak. Can Respir J 2016:8302179. [PubMed: 27610028]

Matsumoto M, Awano H, Ogi M, Tomioka K, Unzaki A, Nishiyama M, Toyoshima D, Taniguchi-Ikeda M, Ishida A, Nagase H, Morioka I, Iijima K. 2016 A pediatric patient with interstitial pneumonia due to enterovirus D68. J Infect Chemother 22:712–715. [PubMed: 27118532]

Messacar K, Abzug MJ, Dominguez SR. 2016 2014 outbreak of enterovirus D68 in North America. J Med Virol 88:739–745. [PubMed: 26489019]

Messacar K, Schreiner TL, Maloney JA, Wallace A, Ludke J, Oberste MS, Nix WA, Robinson CC, Glode MP, Abzug MJ, Dominguez SR. 2015 A cluster of acute flaccid paralysis and cranial nerve dysfunction temporally associated with an outbreak of enterovirus D68 in children in Colorado, USA. Lancet 385:1662–1671. [PubMed: 25638662]

Midgley CM, Jackson MA, Selvarangan R, Turabelidze G, Obringer E, Johnson D, Giles BL, Patel A, Echols F, Oberste MS, Nix WA, Watson JT, Gerber SI. 2014 Severe respiratory illness associated

with enterovirus D68 - Missouri and Illinois, 2014. MMWR Morb Mortal Wkly Rep 63:798–799. [PubMed: 25211545]

Midgley CM, Watson JT, Nix WA, Curns AT, Rogers SL, Brown BA, Conover C, Dominguez SR, Feikin DR, Gray S, Hassan F, Hoferka S, Jackson MA, Johnson D, Leshem E, Miller L, Nichols JB, Nyquist AC, Obringer E, Patel A, Patel M, Rha B, Schneider E, Schuster JE, Selvarangan R, Seward JF, Turabelidze G, Oberste MS, Pallansch MA, Gerber SI, Group E-DW. 2015 Severe respiratory illness associated with a nationwide outbreak of enterovirus D68 in the USA (2014): a descriptive epidemiological investigation. Lancet Respir Med 3:879–887. [PubMed: 26482320]

Muller U, Steinhoff U, Reis LF, Hemmi S, Pavlovic J, Zinkernagel RM, Aguet M. 1994 Functional role of type I and type II interferons in antiviral defense. Science 264:1918–1921. [PubMed: 8009221]

National Research Council (U.S.) Committe for the Update of the Guide for the Care and Use of Laboratory Animals IfLARUS, National Academies Press (U.S.). 2011 Guide for the care and use of Laboratory Animals National Academies Press,

Oberste MS, Maher K, Schnurr D, Flemister MR, Lovchik JC, Peters H, Sessions W, Kirk C, Chatterjee N, Fuller S, Hanauer JM, Pallansch MA. 2004 Enterovirus 68 is associated with respiratory illness and shares biological features with both the enteroviruses and the rhinoviruses. J Gen Virol 85:2577–2584. [PubMed: 15302951]

Palmenberg AC, Gern JE. 2015 Classification and evolution of human rhinoviruses. Methods Mol Biol 1221:1–10. [PubMed: 25261302]

Patel MC, Wang W, Pletneva LM, Rajagopala SV, Tan Y, Hartert TV, Boukhvalova MS, Vogel SN, Das SR, Blanco JC. 2016 Enterovirus D-68 Infection, Prophylaxis, and Vaccination in a Novel Permissive Animal Model, the Cotton Rat (Sigmodon hispidus). PLoS One 11:e0166336. [PubMed: 27814404]

Reed LJ and Muench H. 1938 A simple method of estimating fifty percent endpoints. American Journal of tropical medicine and Hygiene 27:493–197.

Rhoden E, Zhang M, Nix WA, Oberste MS. 2015 In Vitro Efficacy of Antiviral Compounds against Enterovirus D68. Antimicrob Agents Chemother 59:7779–7781. [PubMed: 26149998]

Schuster JE, Miller JO, Selvarangan R, Weddle G, Thompson MT, Hassan F, Rogers SL, Oberste MS, Nix WA, Jackson MA. 2015 Severe enterovirus 68 respiratory illness in children requiring intensive care management. J Clin Virol 70:77–82. [PubMed: 26305825]

Smee DF, Barnard DL. 2013 Methods for evaluation of antiviral efficacy against influenza virus infections in animal models. Methods Mol Biol 1030:407–425. [PubMed: 23821285]

Smee DF, Evans WJ, Nicolaou KC, Tarbet EB, Day CW. 2016 Susceptibilities of enterovirus D68, enterovirus 71, and rhinovirus 87 strains to various antiviral compounds. Antiviral Res 131:61–65. [PubMed: 27063860]

Sun L, Meijer A, Froeyen M, Zhang L, Thibaut HJ, Baggen J, George S, Vernachio J, van Kuppeveld FJ, Leyssen P, Hilgenfeld R, Neyts J, Delang L. 2015 Antiviral Activity of Broad-Spectrum and Enterovirus-Specific Inhibitors against Clinical Isolates of Enterovirus D68. Antimicrob Agents Chemother 59:7782–7785. [PubMed: 26369972]

van den Broek MF, Muller U, Huang S, Aguet M, Zinkernagel RM. 1995 Antiviral defense in mice lacking both alpha/beta and gamma interferon receptors. J Virol 69:4792–4796. [PubMed: 7609046]

Wylie TN, Wylie KM, Buller RS, Cannella M, Storch GA. 2015 Development and Evaluation of an Enterovirus D68 Real-Time Reverse Transcriptase PCR Assay. J Clin Microbiol 53:2641–2647. [PubMed: 26063859]

Zheng HW, Sun M, Guo L, Wang JJ, Song J, Li JQ, Li HZ, Ning RT, Yang ZN, Fan HT, He ZL, Liu LD. 2017 Nasal Infection of Enterovirus D68 Leading to Lower Respiratory Tract Pathogenesis in Ferrets (Mustela putorius furo). Viruses 9(5). pii: E104. [PubMed: 28489053]

Highlights:

- This report describes the first respiratory model for EV-D68 infection in mice.
- This report also describes the process of mouse-adaptation of EV-D68.
- After intranasal inoculation of EV-D68, virus replicates to high titers in the lung and spreads rapidly to other tissues.
- Clinical signs include viremia and disturbances in lung function “enhanced pause” (Penh) by plethysmography.
- Histological lesions show an interstitial pneumonia and lung lavage fluids show increased proinflammatory cytokines.

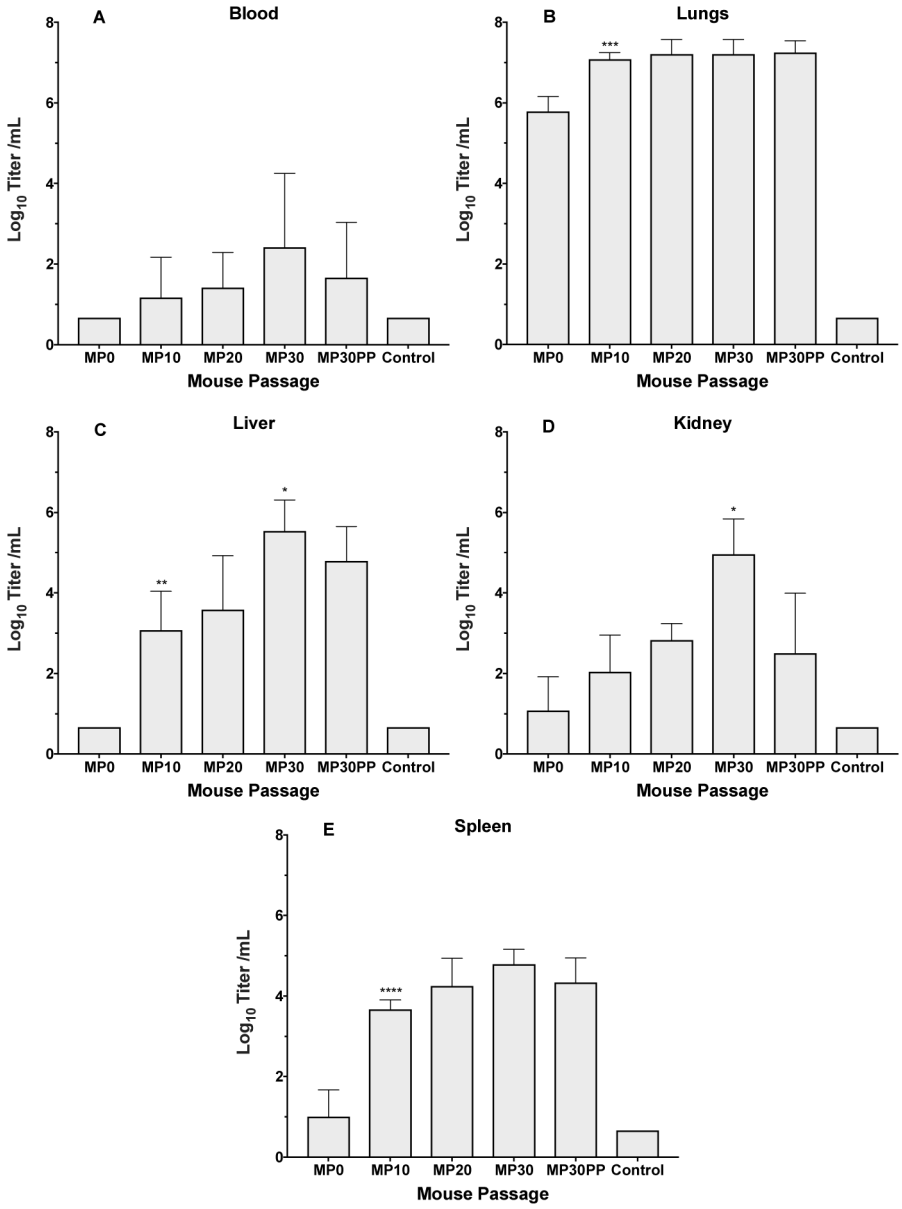

Figure 1: Virus titers in tissues after infection with mouse-adapted EV-D68.

Comparison of virus titers in blood, lungs, liver, kidney and spleen after infection with mouse passaged (MP) viruses. MP30 showed similar significance against MP20 and plaque purified MP30 (MP30pp) virus in kidney tissue. All mice were challenged with 10^6.5 $CCID_{50}$ of the respective viruses in a 90 μl volume. *P<0.05, **P<0.01, ***P<0.001.

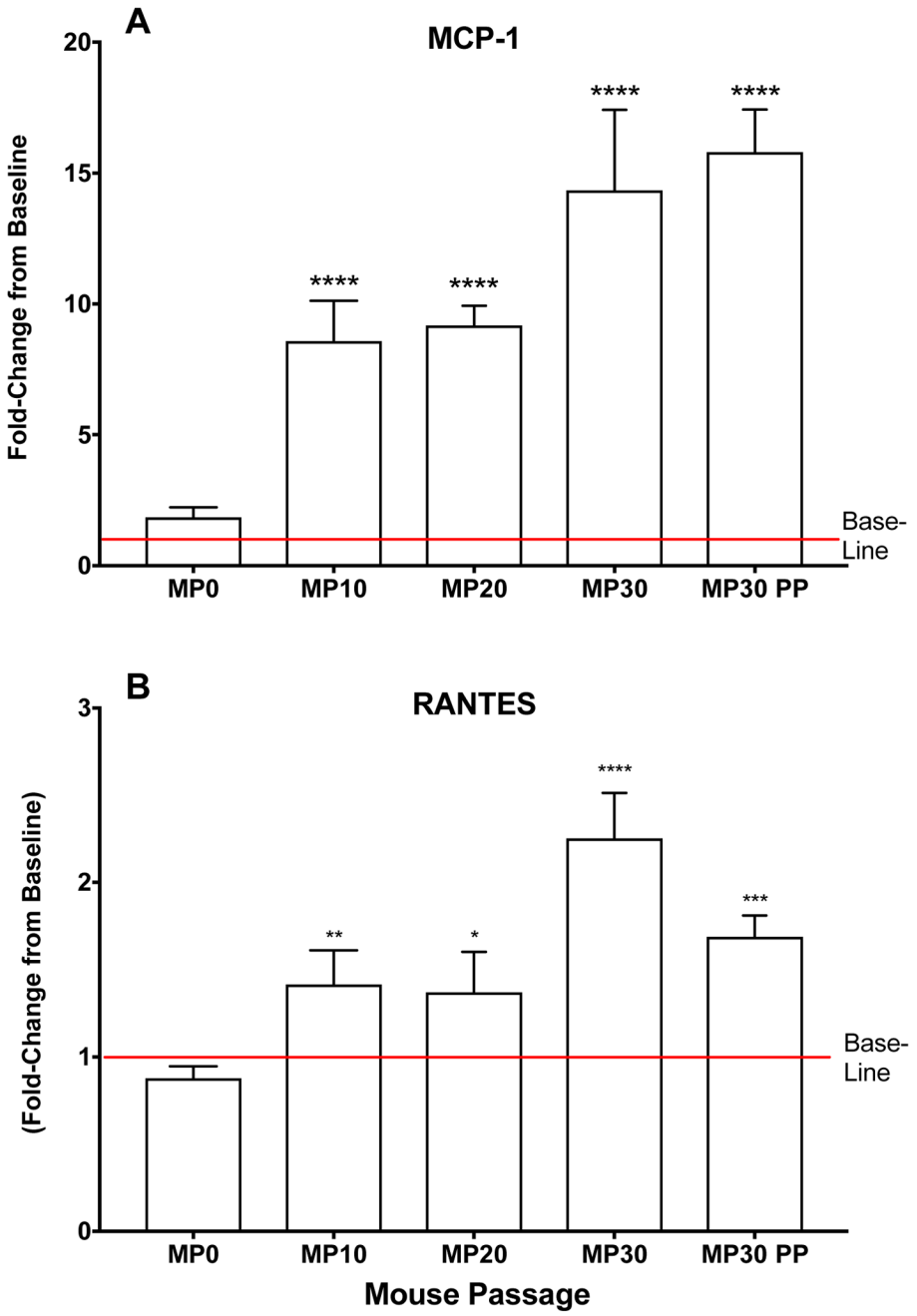

Figure 2: MCP-1 and RANTES in lung homogenates after infection with mouse-adapted EV-D68.

MCP-1 and RANTES values after infection with mouse passaged (MP) viruses. MCP-1 showed the greatest change compared to uninfected mice (baseline) as virus adapted to mice. All mice were challenged with 10^6.5 $CCID_{50}$ of the respective viruses in a 90 μl volume. The values show the average for lung samples collected from mice on day 1 post-virus exposure. *P<0.05, **P<0.01, ***P<0.001, ****P<0.0001.

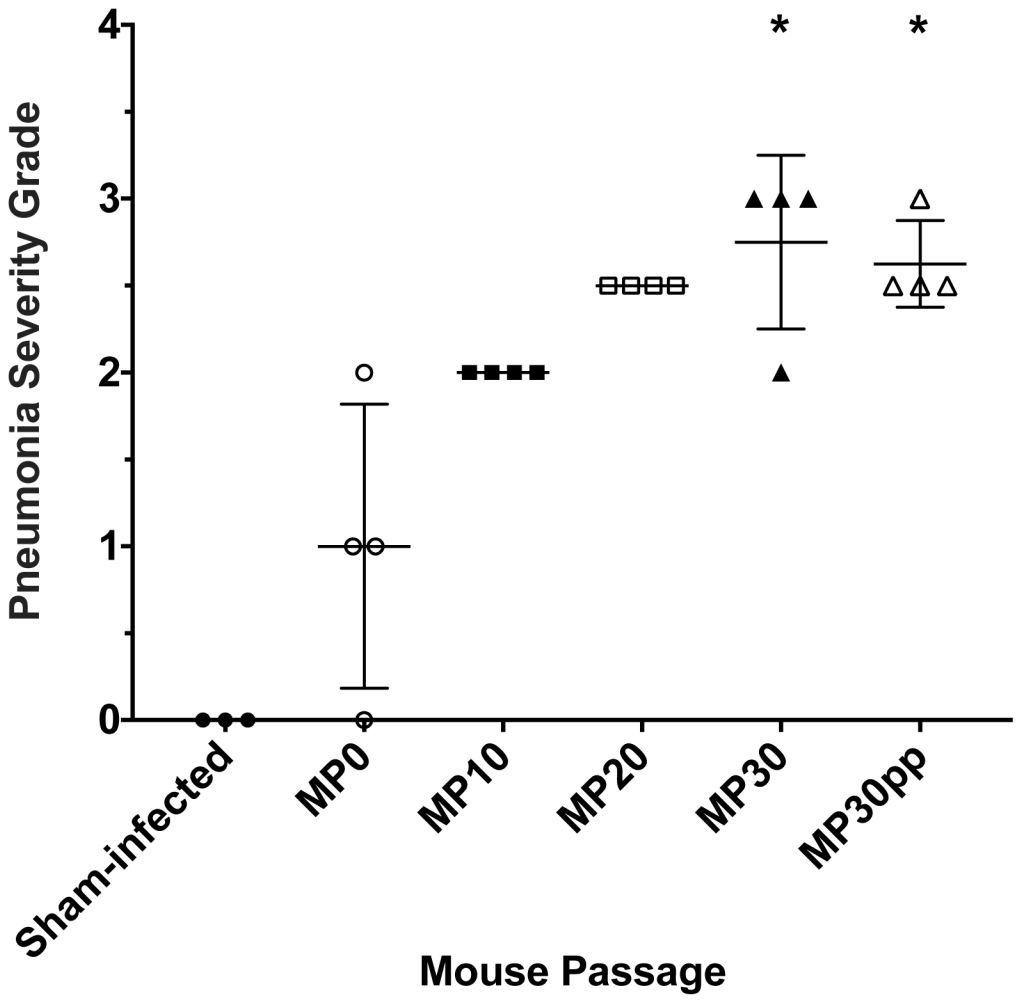

Figure 3: Histologic lesions in lungs after infection with mouse-adapted EV-D68.

All mice were challenged with 10^6.5 $CCID_{50}$ of the respective viruses in a 90 μl volume and sacrificed on day 2 post-infection for histopathology. Groups infected with the mouse passage 30 (MP30) and the MP30 plaque purified (MP30pp) viruses showed significant interstitial pneumonia severity scores compared to sham-infected mice. Each group consisted of 4 mice, except the sham-infected controls, which consisted of 3 mice. *P<0.05 by non-parametric test.

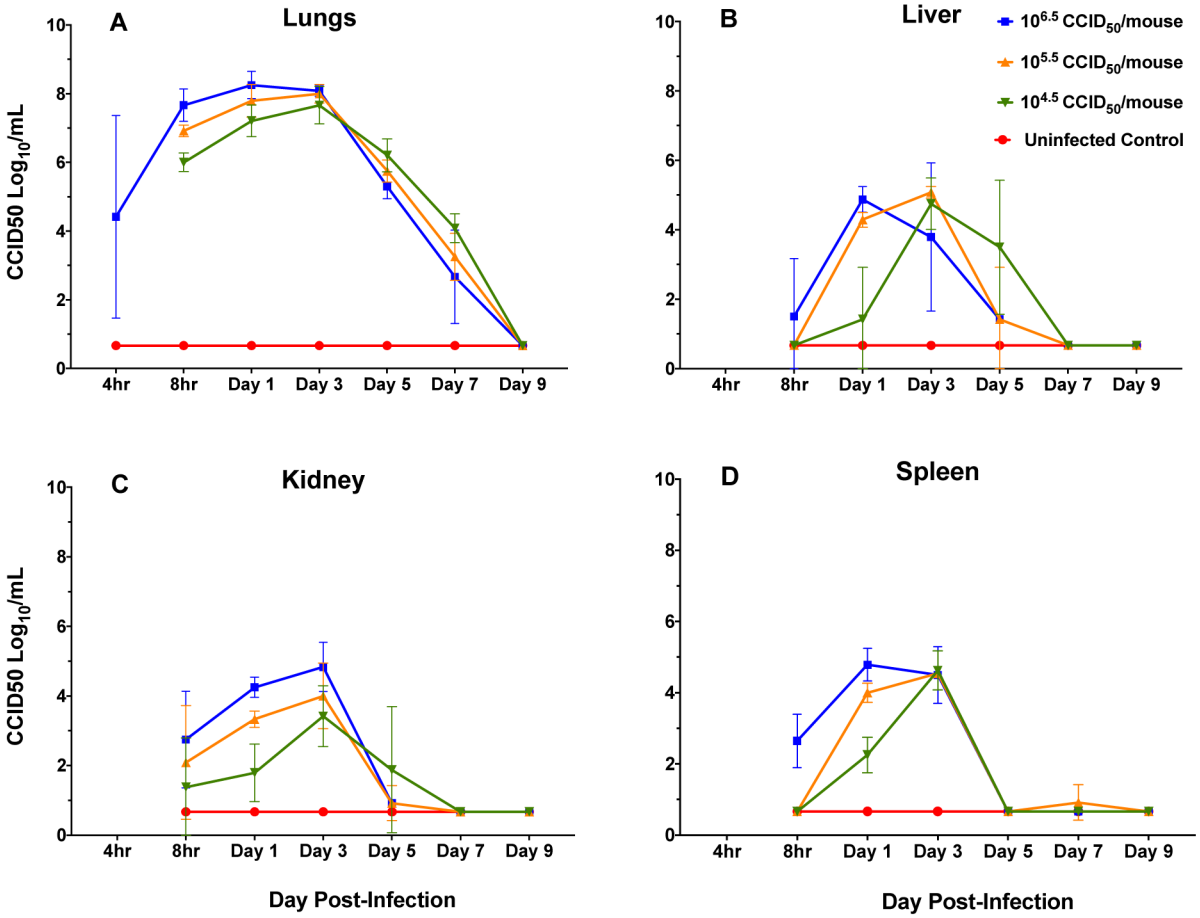

Figure 4: Time course of infection for EV-D68 MP30pp in lungs, liver, kidney and spleen.

Tissues harvested at 4 and 8 hours, then day 1, 3, 5, 7, 9 post-infection with three challenge doses and uninfected (cell culture medium) controls. At each time point, four mice per group were euthanized and tissues collected for virus titration. The group administered the highest challenge dose showed peak virus titers on day 1 for lung, liver, and spleen, and on day 3 for kidney. All other challenge groups showed peak titers on day 3.

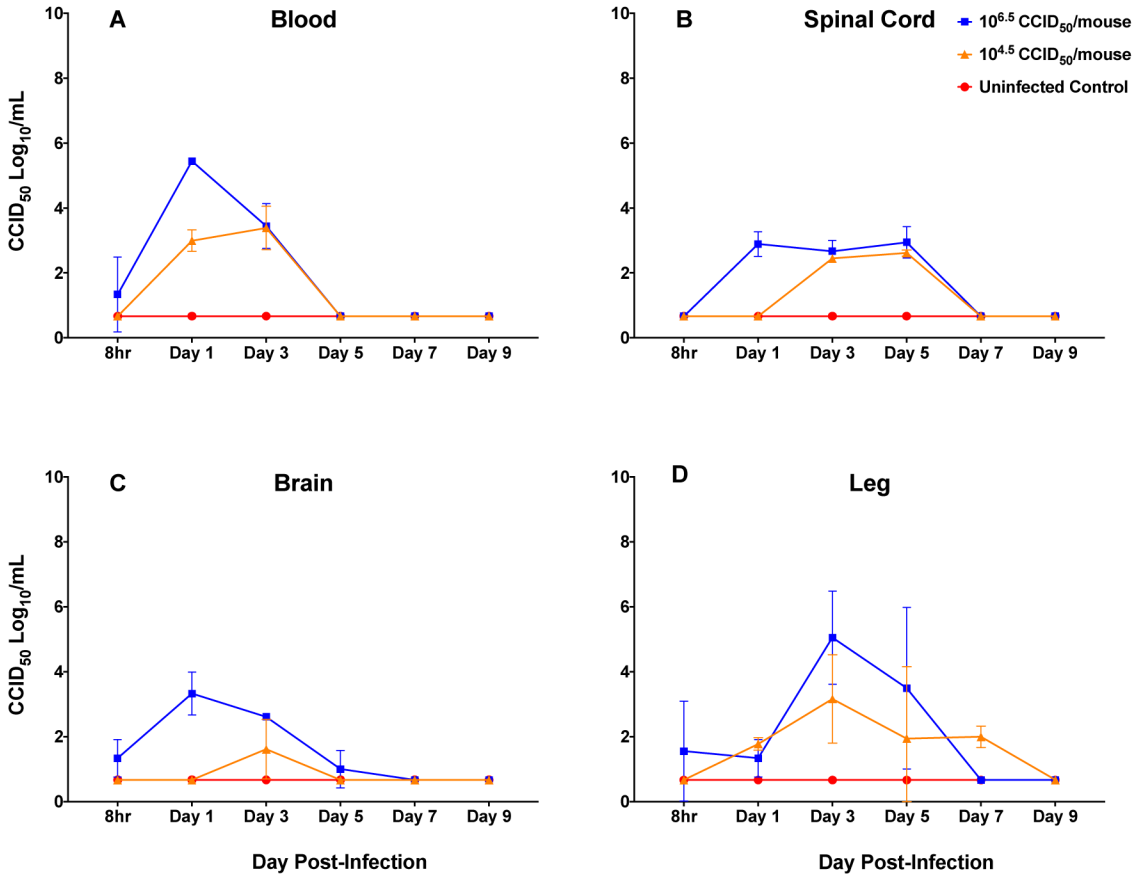

Figure 5: Time course of infection for EV-D68 MP30pp in blood, spinal cord, brain and leg muscle.

Tissues harvested at 8 hours, then day 1, 3, 5, 7, 9 post-infection with two challenge doses and uninfected (cell culture medium) controls. At each time point, four mice per group were euthanized and tissues collected for virus titration. The group administered the highest challenge dose showed peak virus titers on day 1 for blood and brain, and days 1-3 for spinal cord, and on day 3 for leg tissues. The lower dose challenge group showed peak titers on day 3 or 5.

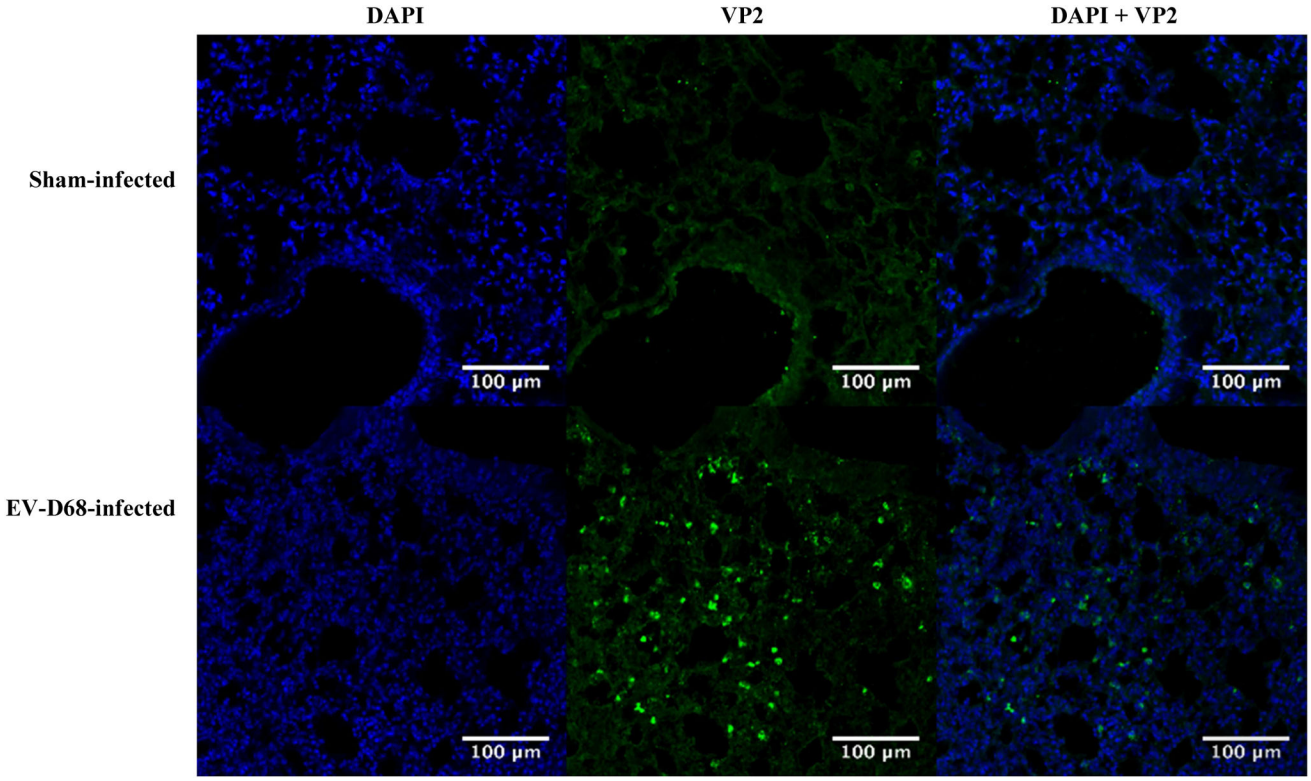

Figure 6: Immunohistofluorescence of EV-D68 MP30pp Infected and sham-infected mouse lungs.

Identification of mouse-passaged, plaque purified (MP30pp) EV-D68 in lung tissues following infection. Comparison of lung sections from sham-infected and virus infected mice on day 2 post-infection, stained for both DAPI (nuclear counterstain) and antibody directed against EV-D68 VP2 capsid protein. Original image overlay has been separated into two images based on wavelength, 405 nm (DAPI) and 488 nm (VP2), for clarity and comparison. A merged image of the two stains is shown on the far right.

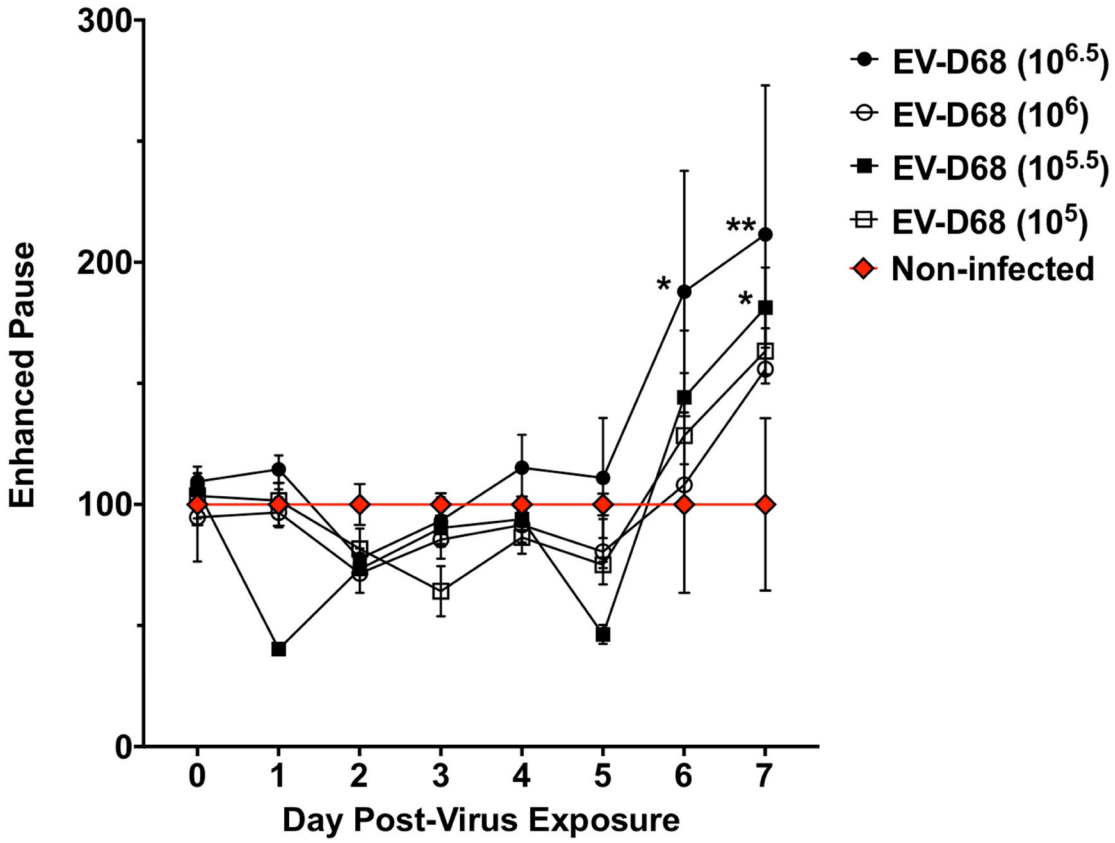

Figure 7: Enhanced pause (Penh) in mice infected with EV-D68 MP30pp.

Four groups of eight mice (4 males and 4 females per group) were used to evaluate the impact of virus challenge on Penh by plethysmography. A non-infected (cell culture medium) control group was used as a baseline for evaluation of lung measurements. After challenge infection, plethysmography readings were obtained daily from days 0-7 post-infection. The group administered the highest challenge dose showed an increase in Penh on days 6 and 7 compared to baseline. *P<0.05

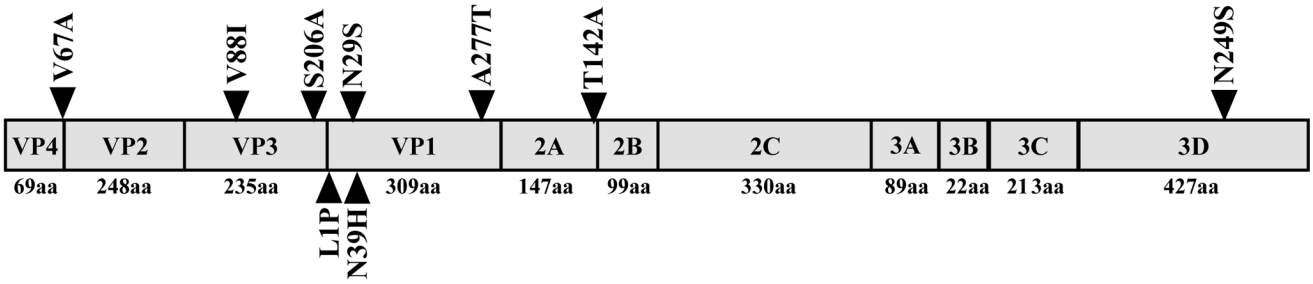

Figure 8: Visual representation of EV-D68 genome and predicted amino acid changes acquired during serial passaging in the lungs of mice.

The polyprotein produced by EV-D68 is shown divided into the final mature peptides. Sizes of each mature peptide are listed below the polyprotein. Locations and predicted amino acid changes are indicated by triangles.

Table 1:

In Vitro Antiviral Activity of EV-D68 MP0, EV-D68 MP30PP and Rhinovirus-14

Compound	No Virus CC_{50} [a]		EV-D68/Missouri (MP0)		EV-D68/Missouri (MP30PP)		Rhinovirus-14	
	RD	Hela-Ohio	EC_{50} [b]	SI [c]	EC_{50} [b]	SI [c]	EC_{50} [b]	SI [d]
Enviroxime	14.1 ± 4.8	22.3 ± 9.7	0.03 ± 0.0	469	0.07 ± 0.03	201	0.13 ± 0.1	108
Pleconaril	10.5 ± 3.5	4.7 ± 2.3	0.08 ± 0.0	131	0.08 ± 0.00	131	0.08 ± 0.0	59.1
Guanidine	1420 ± 315	3030. ± 577	44.7 ± 11.9	31.7	61.0 ± 10.5	23.3	80.7 ± 16.2	37.6
Rupintrivir	>1.0 ± 0.0	>1.0 ± 0.0	0.0003 ± 0.0	>3333	0.0004 ± 0.0001	>2500	0.003 ± 0.0004	>333

Units in μM. Enterovirus D68 tested on RD cells, Rhinovirus-14 tested on Hela-Ohio cells.

[a] 50% cytotoxic concentration (CC_{50}) ± standard deviation from 3 independent experiments.

[b] 50% effective virus-inhibitory concentration ± standard deviation from 3 independent experiments.

[c] SI-Selectivity Index = CC_{50} / EC_{50} using the CC_{50} in RD cells.

[d] SI-Selectivity Index = CC_{50} / EC_{50} using the CC_{50} in Hel-Ohio cells

Table 2:

Summary of nucleotide and predicted amino acid changes after serial passaging of EV-D68 in the lungs of AG129 mice.

Position of Mutation	Nucleotide Change	Predicted Amino Acid Change	Location in Viral Polyprotein
115	G to T	None	5’UTR
136	C to T	None	5’UTR
197	A to G	None	5’UTR
473	G to A	None	5’UTR
634	A to G	None	5’UTR
875	T to C	V67A	VP4
1143	T to C	None	VP2
1888	G to A	V88I	VP3
1935	T to C	None	VP3
2076	T to C	None	VP3
2242	T to G	S206A	VP3
2333	T to C	L1P	VP1
2397	C to T	None	VP1
2417	A to G	N29S	VP1
2446	A to C	N39H	VP1
3160	G to A	A277T	VP1
3390	T to C	None	2A
3682	A to G	T142A	2A
3835	C to T	None	2B
4587	A to G	None	2C
6704	A to G	N249S	3D
7119	A to G	None	3D